AD-A038 532   ROME AIR DEVELOPMENT CENTER GRIFFISS AFB N Y   F/G 17/9
                SIMULATION OF LEADING EDGES OF BACKSCATTER IONOGRAMS FOR IONOSP--ETC(U)
                NOV 76   M S WONG

UNCLASSIFIED   RADC-TR-76-354

                                                                        NL

1 OF 1
AD
A038532

END

DATE
FILMED

5-77

RADC-TR-76-354
IN-HOUSE REPORT
NOVEMBER 1976

Simulation of Leading Edges of Backscatter Ionograms for Ionospheric Inference

MING S. WONG

D D C

APR 22 1977

A

ROME AIR DEVELOPMENT CENTER
AIR FORCE SYSTEMS COMMAND
GRIFFISS AIR FORCE BASE, NEW YORK 13441

This report has been reviewed by the RADC Information Office (OI) and is releasable to the National Technical Information Service (NTIS). At NTIS it will be releasable to the general public, including foreign nations.

APPROVED:

TERENCE J. ELKINS, Chief
Ionospheric Radio Physics Branch
Electromagnetic Sciences Division

APPROVED:

ALLAN C. SCHELL, Acting Chief
Electromagnetic Sciences Division

FOR THE COMMANDER:

REPORT DOCUMENTATION PAGE

READ INSTRUCTIONS
BEFORE COMPLETING FORM

1. REPORT NUMBER	2. GOVT ACCESSION NO.	3. RECIPIENT'S CATALOG NUMBER
RADC-TR-76-354		

4. TITLE (and Subtitle)	5. TYPE OF REPORT & PERIOD COVERED
SIMULATION OF LEADING EDGES OF BACKSCATTER IONOGRAMS FOR IONOSPHERIC INFERENCE	In-House
	6. PERFORMING ORG. REPORT NUMBER

7. AUTHOR(s)	8. CONTRACT OR GRANT NUMBER(s)
Ming S. Wong	

9. PERFORMING ORGANIZATION NAME AND ADDRESS	10. PROGRAM ELEMENT, PROJECT, TASK AREA & WORK UNIT NUMBERS
Deputy for Electronic Technology (RADC/ETEI) Hanscom AFB Massachusetts 01731	61102F 5631 1601

11. CONTROLLING OFFICE NAME AND ADDRESS	12. REPORT DATE
Deputy for Electronic Technology (RADC/ETEI) Hanscom AFB Massachusetts 01731	November 1976
	13. NUMBER OF PAGES
	23

14. MONITORING AGENCY NAME & ADDRESS(if different from Controlling Office)	15. SECURITY CLASS. (of this report)
23p.	Unclassified
	15a. DECLASSIFICATION/DOWNGRADING SCHEDULE

16. DISTRIBUTION STATEMENT (of this Report)

Approved for Public Release; Distribution Unlimited.

17. DISTRIBUTION STATEMENT (of the abstract entered in Block 20, if different from Report)

18. SUPPLEMENTARY NOTES

19. KEY WORDS (Continue on reverse side if necessary and identify by block number)

Swept-frequency backscatter ionograms
Backscatter-ionogram synthesis
Electron-density distribution, HF Propagation
Backscatter-ionogram inversion

20. ABSTRACT (Continue on reverse side if necessary and identify by block number)

Jones' ray-tracing program and integrated subroutines by Langworthy and Barrett are being used to compute swept-frequency ionograms, for backscatter by ground and field-aligned ionization, in the presence of sharp horizontal boundaries in electron-density distributions. Prominent characteristics, minimum group-path traces, ray-density variations, and off-great-circle deviation along ray paths are presented for various alterations on major features of initial electron distributions.

DD FORM 1473 EDITION OF 1 NOV 65 IS OBSOLETE
1 JAN 73

Unclassified

309050

20. Abstract (Continued)

An arbitrary distribution is encoded, and successively varied, with a piecewise representation that is easy for the user and free from unintended, fluctuating deviations at spatial points away from the set of given data points. This is imperative for inference, starting with an observed backscatter ionogram, of electron-distribution features by means of iterative ionogram computations.

Preface

The results of computations presented in this report were obtained with the CDC 6600 Computer at the Air Force Geophysics Laboratory, and with computer programs developed by Dr. T. Barrett and Mrs. B. Langworthy of Parke Mathematical Laboratories, for backscatter-ionogram synthesis and display. Deeply appreciated are their contributions, and also the advice and support of Dr. T. Elkins, Chief of the Ionospheric Radio Physics Branch.

3

Contents

Illustrations

6

Simulation of Leading Edges of Backscatter Ionograms for Ionospheric Inference

1. INTRODUCTION

This report presents the results of ray computations made for simulating the principal features of swept-frequency backscatter radar ionograms, with emphasis on the leading-edge traces appearing in such ionograms. The eventual objective is to infer, from observed backscatter-radar ionograms, important features of the ionospheric electron-density distribution in the observational sector of the radar, and thereby infer the major effects of the ionosphere upon the performance of the radar. The eventual procedure is to start with an initially assumed, trial electron distribution, and then iteratively alter the electron distribution until the computed leading-edge traces approximately match the corresponding traces in the given set of observed backscatter ionograms.

The ray computations were made under conditions of three-dimensional variations in the ionosphere at polar latitudes. Figure 1 shows a shaded area where auroral activity and field-aligned ionization were observed near local midnight hours on 9 December 1971. (The southern edge of the shaded area constitutes the southern boundary[1] of the auroral oval.) At this time, the center line-of-sight of

1. Buchau, J., Pike, C.P., and Wong, M.S. (1973) Detailed Specification of the Arctic Ionosphere and an Application to Three-Dimensional Ray Tracking, AFCRL-TR-73-0726.

the radar grazed the boundary between the aurorally active and F-layer trough regions. In this situation, it is to be expected that the radar antenna beam along the center line-of-sight azimuth would experience strong off-great-circle deviations.
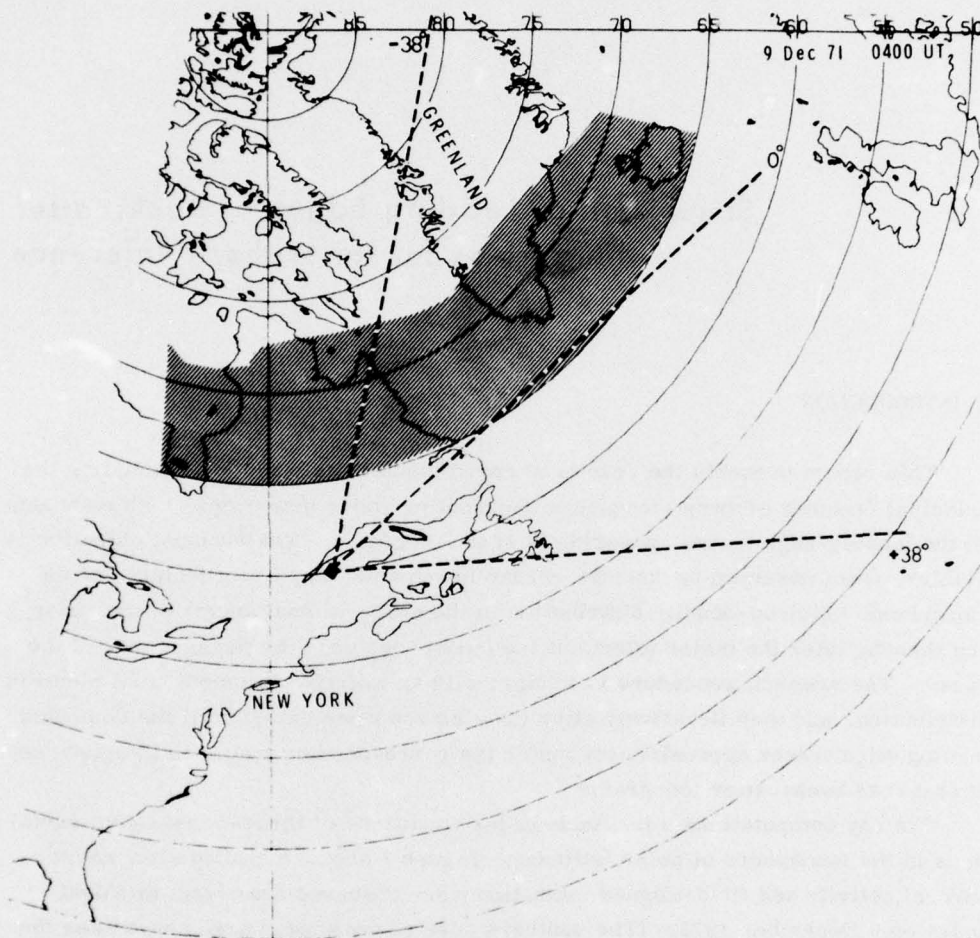

Figure 1. Lines of Sight from Backscatter Radar, and Location of Field-aligned Ionization Observed in Shaded Area near 2300 LT on 9 December 1971. (After Buchau et al.) The map is plotted in accurate geomagnetic latitude and longitude

2. REPRESENTATION AND ALTERATION OF ELECTRON-DENSITY DISTRIBUTIONS

In ray computations using the Jones program[2] for solving Hamiltonian ray equations for anisotropic media, the dipolar geomagnetic coordinate system is most advantageously used. As seen in Figure 1, accurate geomagnetic coordinates are appropriate for describing important ionospheric features at polar latitudes. Thus, it is necessary to use the geographic, the dipolar-geomagnetic, and the accurate-geomagnetic systems of coordinates interchangeably in ray and ionogram computations.

Figure 2 shows the transformation between geographic and accurate-geomagnetic coordinates.[3] The contours of geographic colatitude are shown in 1-degree increments. Origin of the accurate geomagnetic (polar) coordinates is at the intersection of the row and column of dots spaced at 5-degree increments of geomagnetic colatitude. Figure 3 shows the transformation between dipolar-geomagnetic and accurate-geomagnetic coordinates. The curves in Figure 3 were obtained by using a computer subroutine developed by Bhavnani[4] for inverting the Gustafsson tables,[5] which converts geographic to accurate-geomagnetic coordinates, and by using a transformation matrix between geographic and dipolar-geomagnetic coordinates.

For convenience, as in a previous report,[6] an arbitrary electron distribution is deliberately taken to consist of one part extending over the entire geographic region of interest, and a second part over a smaller area (for example, strong E-layer ionization over latitudinal and longitudinal intervals associated with auroral activities). For each of these two parts, the electron density varies with height as a continuous sequence of up to five monotonic segments in the bottom side of the ionosphere; each segment is a sine-squared function with zero slopes at the ends, increasing or decreasing with altitude. The Chapman function is used for the top side of the ionosphere.

2. Jones, R.M., and Stephenson, J.J. (1975) A Three-Dimensional Ray Tracing Computer Program for Radio Waves in the Ionosphere, OT Report 75-76, U.S. Department of Commerce, Office of Telecommunications. (For sale by Government Printing Office.)

3. Whalen, J.A. (1970) Auroral Oval Plotter and Nomograph for Corrected Geomagnetic Local Time, Latitude, and Longitude, AFCRL-TR-70-0422.

4. Bass, J.N., and Bhavnani, K.H. (1974) Analysis and Programming for Scientific Research, AFCRL-TR-74-0480.

5. Gustafsson, G. (1970) A revised corrected geomagnetic coordinate system, Arkiv Geofysik 5:595-617.

6. Wong, M.S. (1975) Iterative Ray-Tracing Simulation of Minimum Group-Path Traces in Swept-Frequency Backscatter Ionograms, AFCRL-TR-75-0241.
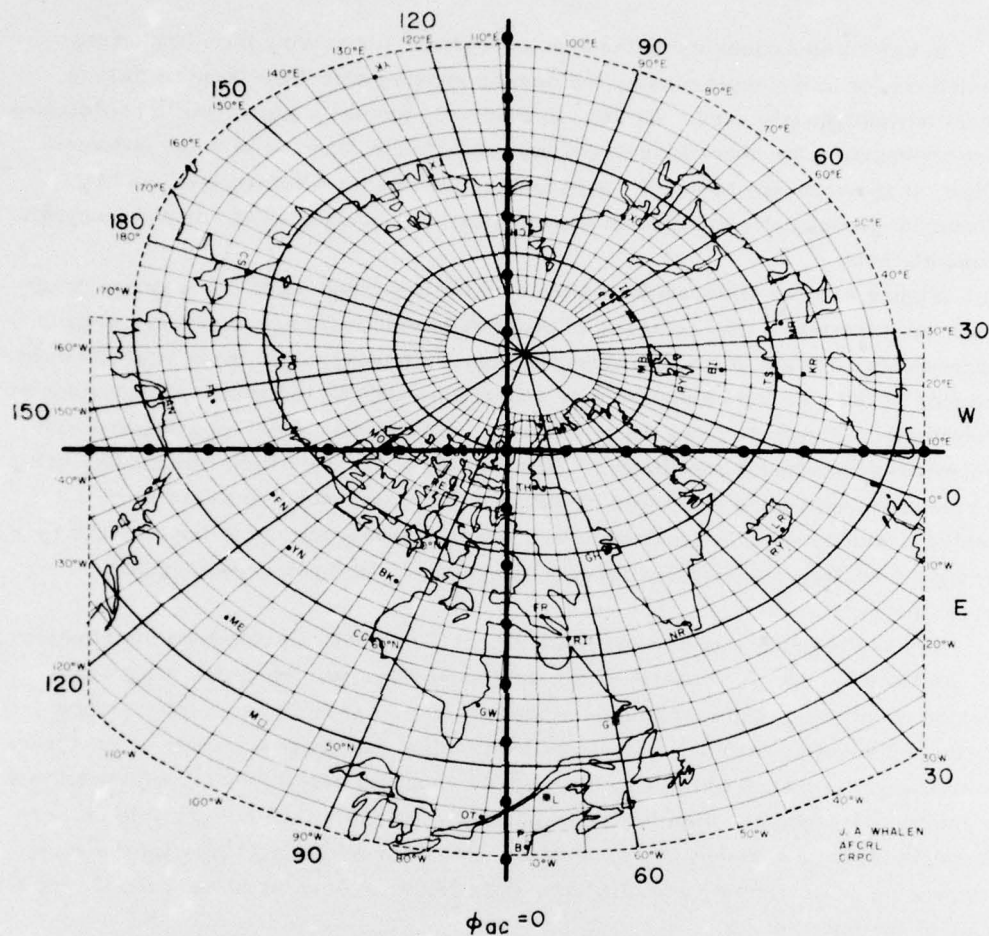
$\phi_{ac} = 0$

Figure 2. Curves of Geographic Colatitudes and Longitudes Plotted on Polar Co-ordinates for Accurate Geomagnetic Latitude and Longitude. (After Whalen.)

Figure 4 illustrates how the sine-squared segments may be used for the two parts of the electron distribution. For each segment, the maximum and minimum electron densities, as well as their altitudes, all may be functions of colatitude θ_{ac} in the accurate geomagnetic coordinate system. As shown in Figure 5a, each function of θ_{ac} consists of a continuous sequence of sine-squared function segments with zero slopes at the end points of each segment.
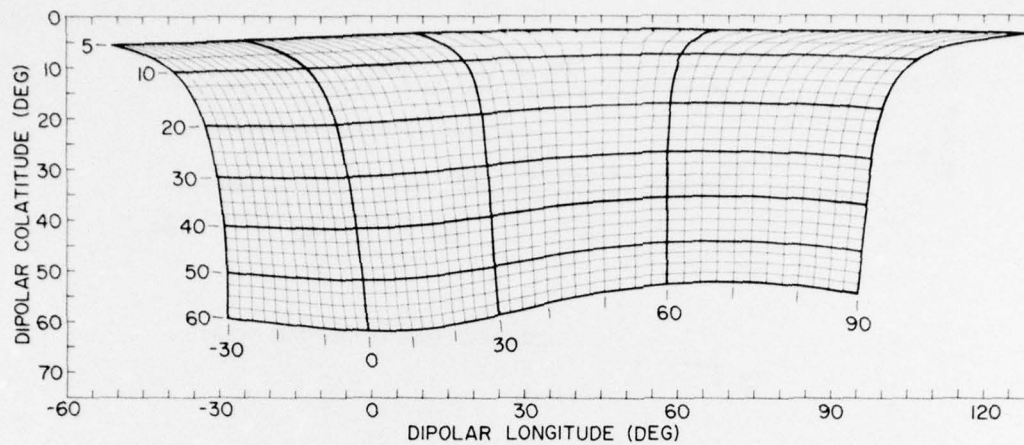
10

Figure 3. Curves of Accurate Geomagnetic Latitudes and Longitudes Plotted on Cartesian Coordinates for Dipolar Geomagnetic Latitude and Longitude
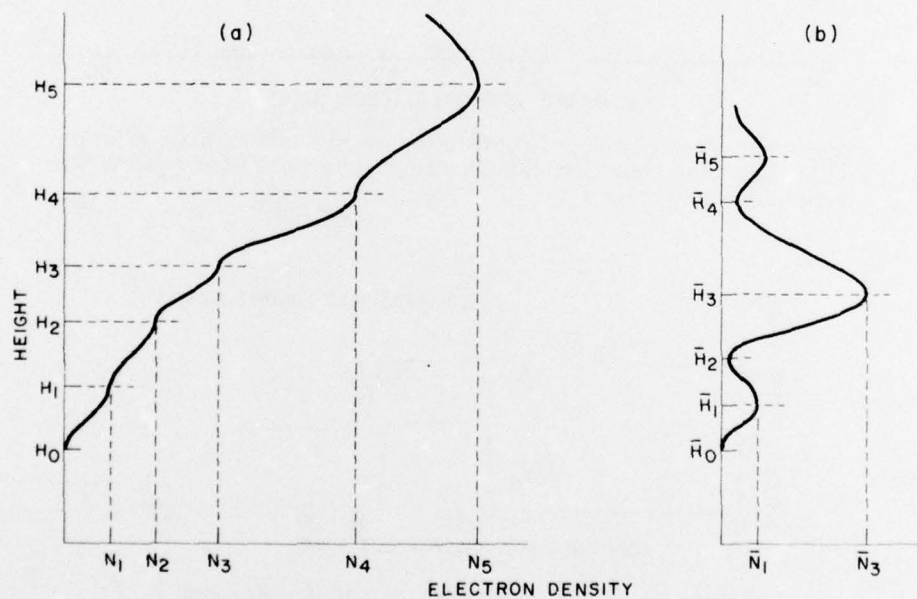

Figure 4. Two Separate Electron-density vs Height Profiles Used for Representing any Given Electron Distribution. Each profile consists of five sine-squared segments joined continuously for bottom side of ionosphere
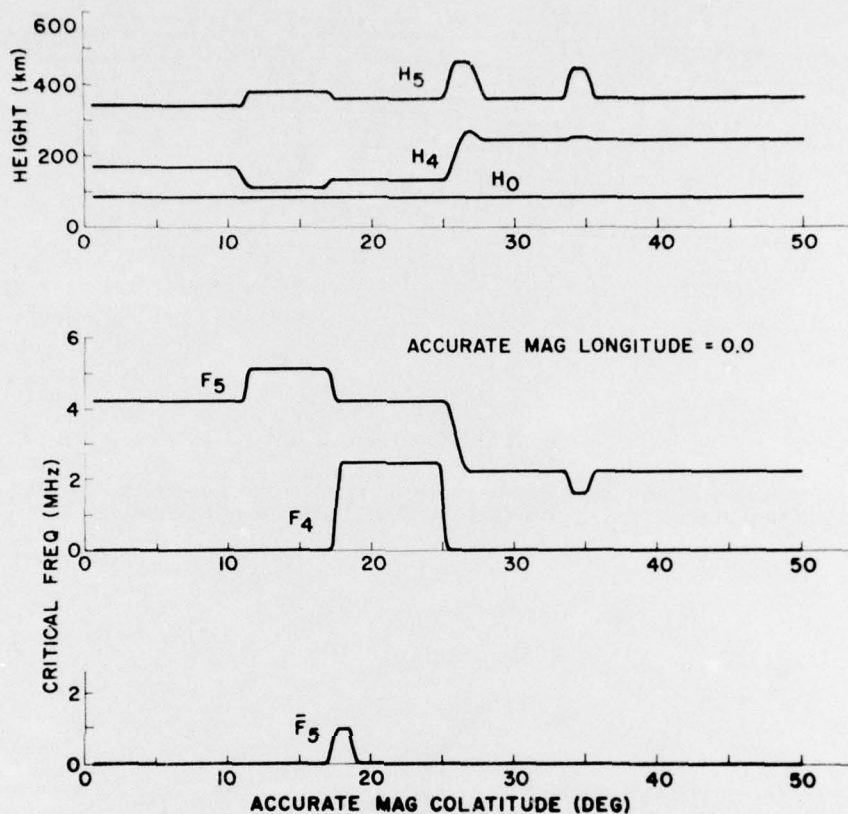
11

Figure 5a. Variation with Accurate Geomagnetic Colatitude of Critical Frequencies, and Critical-frequency Heights of Sine-square Segments Shown in Figure 4

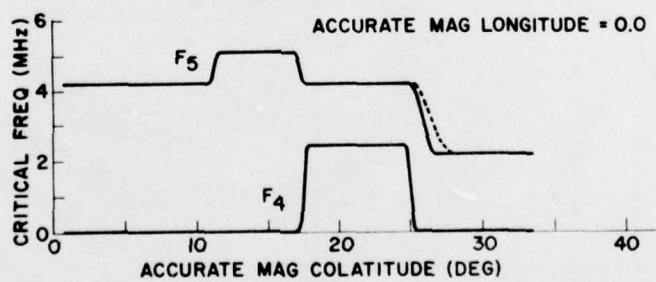Figure 5b. An Alteration of the Critical-frequency Function F_5 in Figure 4 with the Dash-line Segment Replacing the Original, Steeper Solid-line Segment

12

Figure 6. The Critical Frequencies and Heights F_4, F_5, $\overline{F}_5$, H_4 and H_5 in Figure 5 Plotted as Functions of Ground Range from the Backscatter Radar in Various Azimuths: (a) 20° and 25°; (b) 30° and 35°; (c) 40° and 45°; (d) 50° and 55°
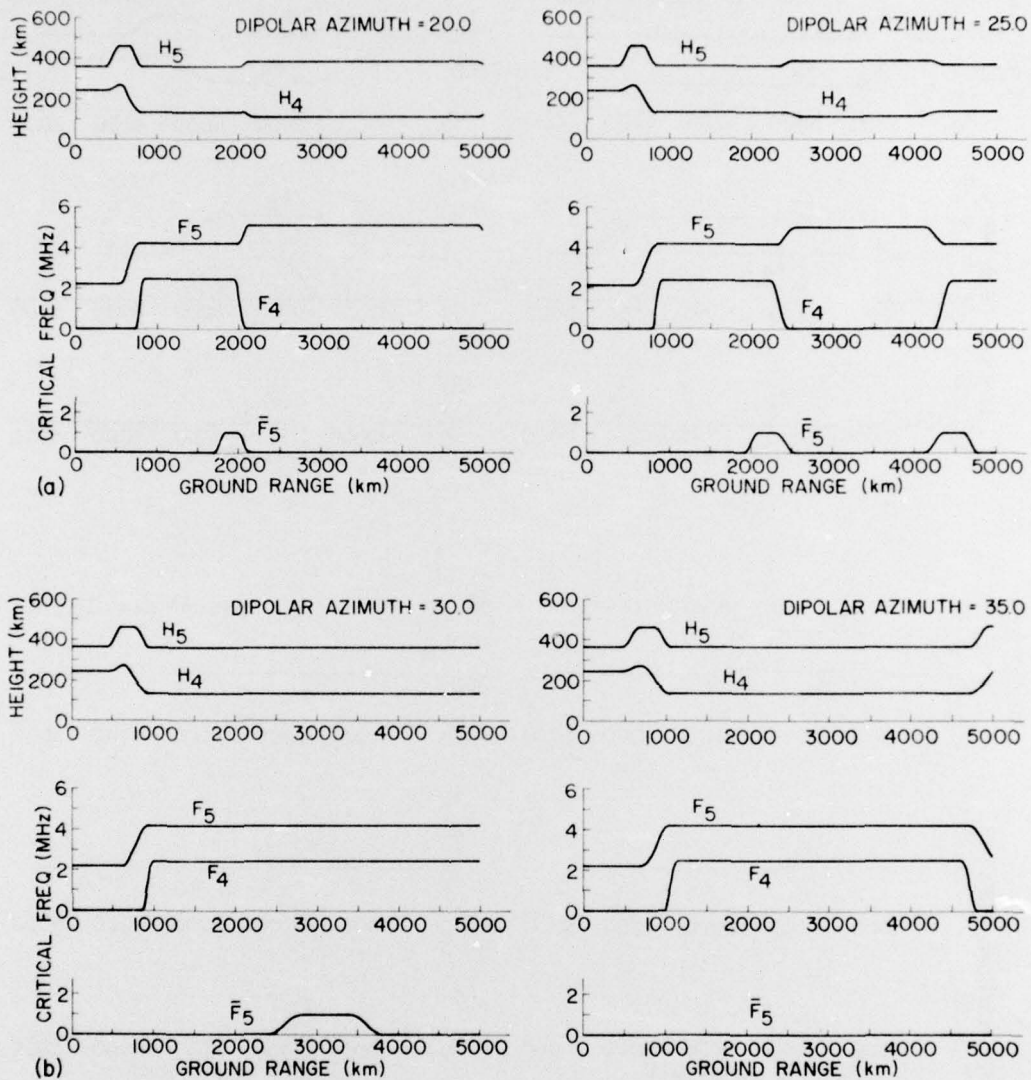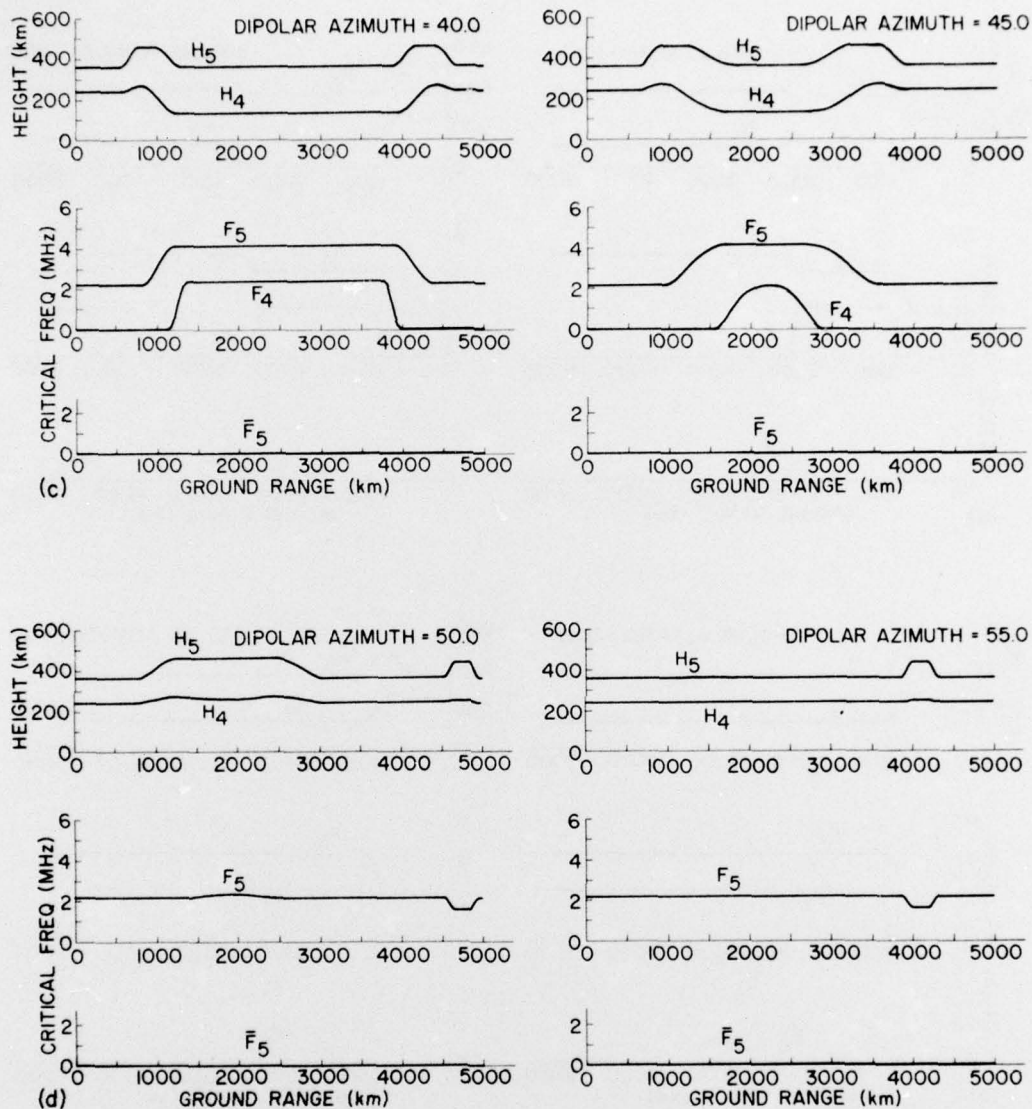
13

Figure 6. The Critical Frequencies and Heights F_4, F_5, $\bar{F}_5$, H_4 and H_5 in Figure 5 Plotted as Functions of Ground Range from the Backscatter Radar in Various Azimuths: (a) 20° and 25°; (b) 30° and 35°; (c) 40° and 45°; (d) 50° and 55° (Cont.)

For the results presented in the report, the curves in Figure 5a were taken to remain unchanging over a 90-degree sector in accurate geomagnetic longitude ϕ_{ac} for local times near midnight. However, the electron-density processing sub-routine used does include provisions for perturbational variations with ϕ_{ac} of the curves in Figure 5a. [7]

Figure 5b shows an example of the major-feature alterations that can be made very expeditiously, using an electron-density preprocessing subroutine,[7] on the function $F_5(\theta)$ appearing in Figure 5a.

Viewed as functions of ground range from the transmitter at $(\theta_o, \phi_o) = (32.0, 1.8)$ degrees, and in various chosen directions of initial ray azimuth reckoned in the dipolar-geomagnetic coordinate system, the curves in Figure 5a become transformed to those in Figures 6a, b, c, and d.

3. COMPUTED-IONOGRAM CHARACTERISTICS

For the electron-density distribution N($\underline{r}$) represented by Figures 4 and 5a, ray trajectories were computed for various initial take-off angles in elevation, and with frequency and initial azimuth as parameters. Azimuth, colatitude θ, and longitude ϕ are all reckoned in the dipolar geomagnetic system of coordinates in this section.

Figure 7 shows the group-path lengths of rays from the transmitter to back-scattering points either in a field-aligned region where the wave-normal directions intercept the accurate geomagnetic field vector at 90.0 degrees in aspect angle, or in a landing area of the rays at ground level. The curves were computed with the transmitter at $(\theta_o, \phi_o) = (32.0, 1.8)$ degrees, for frequency = 5.75 MHz, and for initial azimuths of the rays at 10, 15, ... 55 degrees. The larger (underlined) numbers near the slanting U-shaped curves denote initial azimuths; the smaller numbers denote initial elevation angles of the rays concerned. The horizontal axis represents the azimuths of back-scattering points viewed from the transmitter.

In Figure 7, the rays emitted at one azimuth are divided typically into sub-intervals of initial elevation angle. Each subinterval gives rise to a slanting U-shaped diagram; more than one U-shaped diagram may belong to one single propagation mode, such as one-hop E, one-hop F, backscatter by field-aligned ionization, or combination of these modes. Thus there may be more than one group-path minimum for rays emitted in a single azimuth and propagated via a single mode. These group-path minima, plotted as functions of frequency, in turn give rise to multiple "leading-edge" traces for a single propagation mode in

7. Langworthy, B., and Barrett, T. (1976) Final Report under Contract F19628-76-C-0029, RADC/ET, Hanscom AFB.
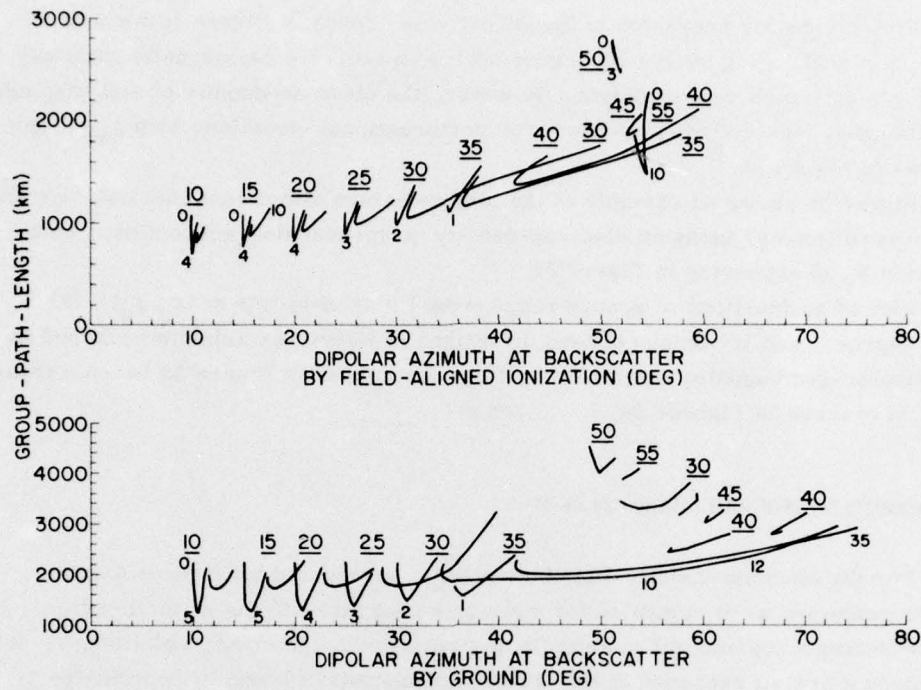
Figure 7. Group-path Lengths for Rays Transmitted at Various Take-off Angles of Elevation and at Fixed Initial Azimuths, Plotted Against the Azimuths at the Backscattering Points of the Rays Concerned. Initial azimuths = 10°, 15°, ... 55°; transmitter at $(32^O, 1.8^O)$; frequency = 5.75 MHz; N(r) shown in Figures 4 and 5a. Bottom half for ground backscatter; top half for backscatter by field-aligned ionization

observed backscatter-radar ionograms. For each point on a U diagram, the backscatter azimuth minus the initial ray azimuth measures the off-great-circle path deviation of the backscatter points concerned from the initial ray azimuth; a negative difference indicates a clockwise deviation in azimuth. Off-great-circle deviations of more than -20 degrees occur for some rays. However, for rays near the group-path minimum in a U diagram (that is, rays which have nearly maximum ray density), the deviation is typically a few degrees.

Figures 8, 9, and 10 show the leading-edge (minimum group-path) traces obtained with the transmitter at $(\theta_O, \phi_O) = (32.0, 1.8)$, $(34.0, 1.8)$, and $(36.0, 1.8)$ degrees respectively, and for various initial ray azimuths between 20 and 50 degrees. The propagation modes involved in the curves shown are ground backscatter via the E or F region (labeled EG, or FG); and backscatter by field-aligned ionization in the E or F region (EI, or FI), at points where the aspect angle between the wave-normal direction of the ray, and the direction of the accurate geomagnetic-field vector is 90°. The curves drawn with dashes indicate that the initial elevation
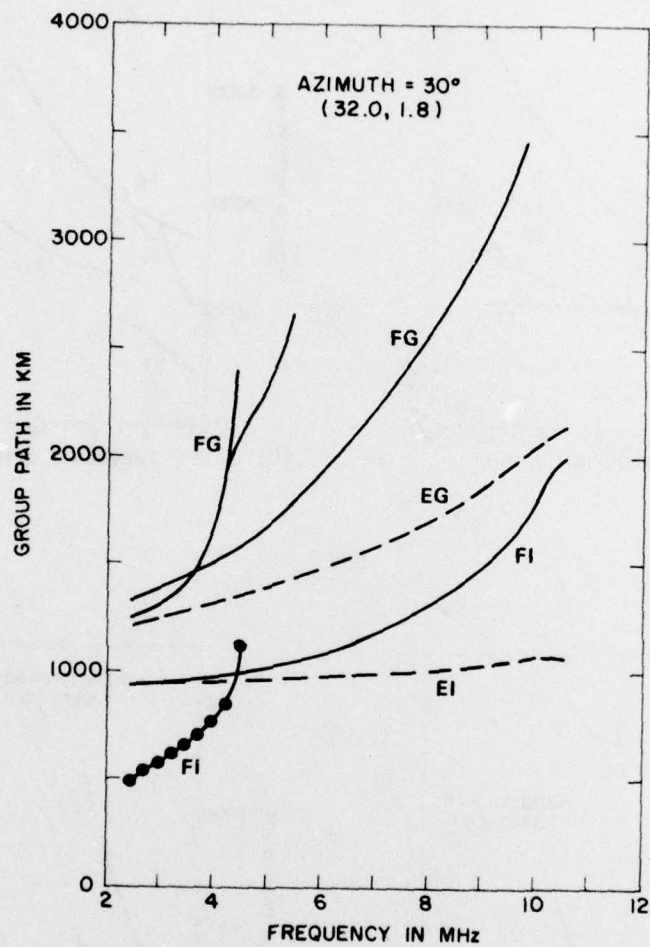
16

AZIMUTH = 30°
(32.0, 1.8)

Figure 8. Computed Leading-edge Traces for N(r) Shown
in Figures 4 and 5a. Transmitter at (32°, 1.8°), and
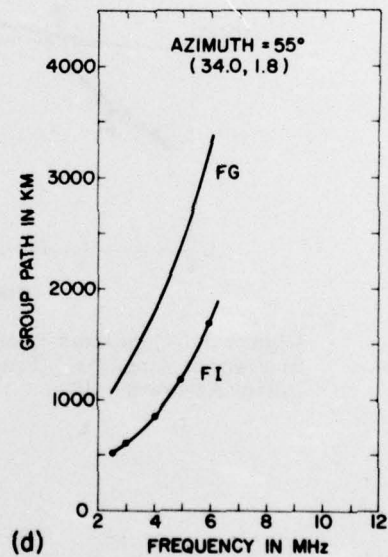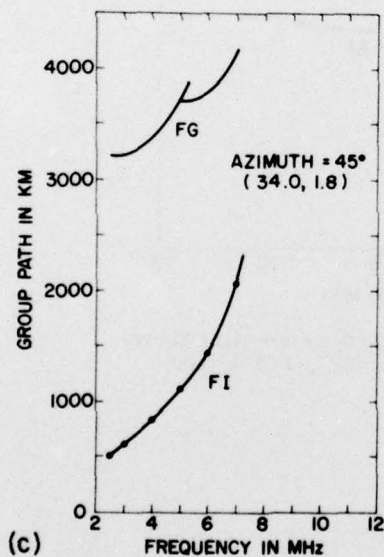Initial Azimuth = 30°
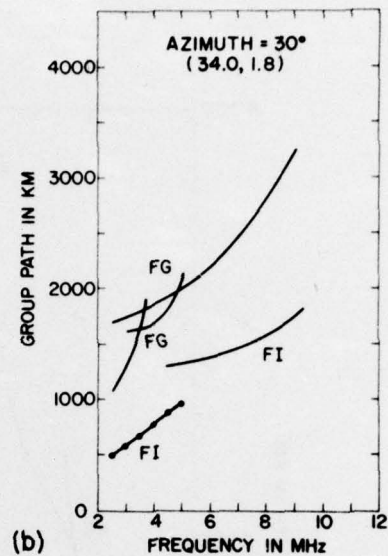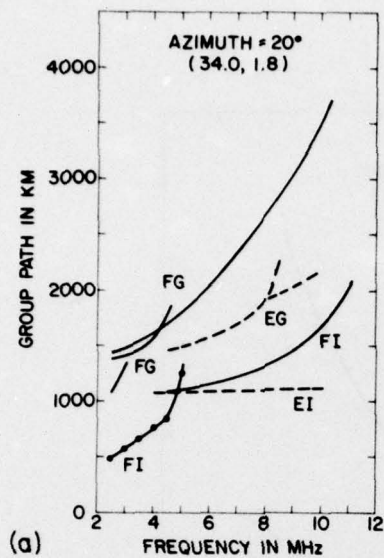
17

Figure 9. Leading-edge Traces for N(r) Shown in Figures 4 and 5a. Transmitter at $(34^\circ, 1.8^\circ)$; (a) initial az = 20°; (b) initial az = 30°; (c) initial az = 45°; (d) initial az = 55°

18

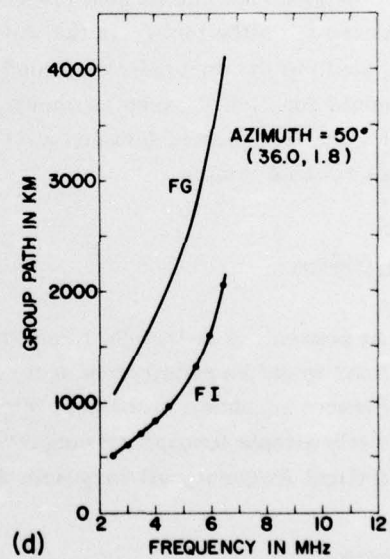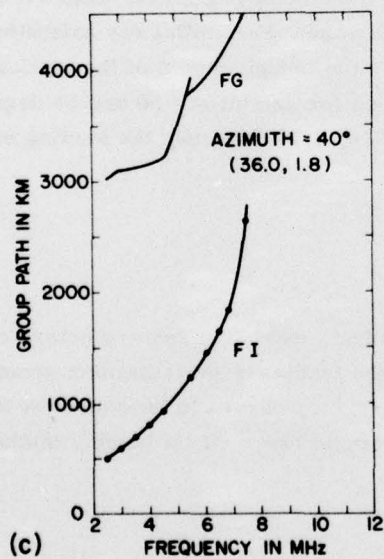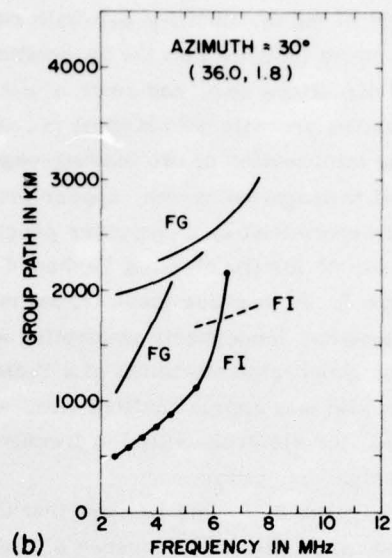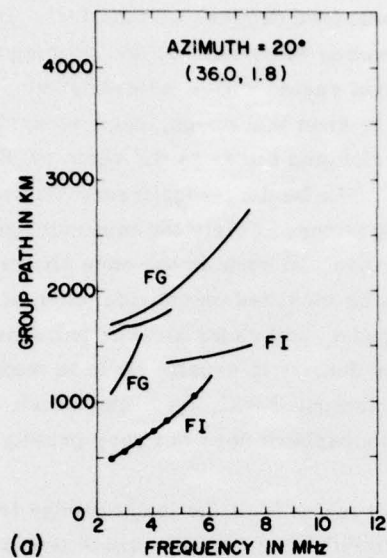Figure 10. Leading-edge Traces for N(r) Shown in Figures 4 and 5a; (a) initial az = 20°; (b) initial az = 30°; (c) initial az = 40°; (d) initial az = 50°

19

angles of the minimum-group-path rays are small (two degrees or smaller). Dots on a curve indicate that the perpendicularity between wave-normal and geomagnetic-field directions occurred south of the auroral oval region where field-aligned ionization prevails with highest probability. It is seen that cusps, each occurring at the intersection of two leading-edge traces belonging either to the same or different propagation modes, appear prominently. The leading-edge traces shown were determined by a computer program that considered solely the minimum group path length for the slanting U-shaped diagrams involved such as the ones shown in Figure 7. In practice these traces may need to be modified on consideration of ray density, ionospheric absorption along ray paths, and radar antenna patterns. At the group-path minimum of a U diagram, ray density is usually close to maximum with fair approximation; also, absorption computed with the Elkins-Rush model[8] for electron-collision frequency in the ionosphere does not vary greatly for neighboring rays.

Figures 8, 9, and 10 show that the principal features of the leading-edge traces change gradually with increase of initial ray azimuth until the rays graze the latitudinal belt shown in Figure 5a where the critical frequency F_5 falls steeply with geomagnetic colatitude. Then the leading-edge traces for the E-region propagation modes disappear, because in Figure 5a, the E-region ionization vanishes south of the auroral-oval, and F-layer propagation modes have their maximum frequencies reduced. Also, the rays which graze the auroral-oval boundary region at F-layer heights experience the largest off-great-circle deviations (clockwise when viewed downward from the top) from the initial ray azimuths. For initial ray azimuths lying south of the auroral-oval boundary, and in the trough region of the critical-frequency function F_5 such as shown in Figure 6d for azimuths = 50 and 55 degrees, and for the transmitter location at $(\theta_o, \phi_o) = (32.0, 1.8)$ degrees, the leading edge traces become simple.

4. DISCUSSION

At present, it is thought likely that, in general, extensive ray-trajectory computations would be required in order to obtain the leading-edge (minimum group-path) traces as shown in the preceding section. This appears to be true even for a relatively simple ionosphere consisting of one single layer, if its height, thickness and critical frequency all vary with distance.

---

8. Rush, C.M., and Elkins, T.J. (1975) An assessment of the magnitude of the F-region absorption on HF radio waves using realistic electron density and collision frequency models, ITU Telecommunication Journal, 1-13.

To infer the principal features of an electron-density distribution over a large region by means of starting with a trial distribution, and then proceeding by iterative computation of leading-edge traces, a considerable number of successive alterations of the initial trial distribution would need to be made before the computed leading-edge traces can be brought to acceptable agreement with the corresponding traces in an observed backscatter ionogram.

For this procedure of iterative computation of leading-edge traces to be generally useful, two conditions are involved. First, faster ray computation needs to be developed. Now it requires approximately 0.5 hours or more of Central Processor time with the very fast CDC 6600 Computer in order to obtain the leading-edge traces for one initial ray azimuth. Second, the procedure is workable provided that when the initial trial electron distribution is successively altered in some monotonic fashion, the resulting successive sets of leading-edge traces are also altered in a monotonic fashion within a common frequency interval at middle-range frequencies where the traces persist and are relatively free from complicating cusps or irregularities. When this second condition is met, multiple-regression techniques can be used to determine the optimal electron-distribution being sought.

References

1. Buchau, J., Pike, C.P., and Wong, M.S. (1973) Detailed Specification of the Arctic Ionosphere and an Application to Three-Dimensional Ray Tracking, AFCRL-TR-73-0726.

2. Jones, R.M., and Stephenson, J.J. (1975) A Three-Dimensional Ray Tracing Computer Program for Radio Waves in the Ionosphere, OT Report 75-76, U.S. Department of Commerce, Office of Telecommunications. (For sale by Government Printing Office.)

3. Whalen, J.A. (1970) Auroral Oval Plotter and Nomograph for Corrected Geomagnetic Local Time, Latitude, and Longitude, AFCRL-TR-70-0422.

4. Bass, J.N., and Bhavnani, K.H. (1974) Analysis and Programming for Scientific Research, AFCRL-TR-74-0480.

5. Gustafsson, G. (1970) A revised corrected geomagnetic coordinate system, Arkiv Geofysik 5:595-617.

6. Wong, M.S. (1975) Iterative Ray-Tracing Simulation of Minimum Group-Path Traces in Swept-Frequency Backscatter Ionograms, AFCRL-TR-75-0241.

7. Langworthy, B., and Barrett, T. (1976) Final Report under Contract F19628-76-C-0029, RADC/ET, Hanscom AFB.

8. Rush, C.M., and Elkins, T.J. (1975) An assessment of the magnitude of the F-region absorption on HF radio waves using realistic electron density and collision frequency models, ITU Telecommunication Journal, 1-13.

MISSION
of
Rome Air Development Center

RADC plans and conducts research, exploratory and advanced development programs in command, control, and communications (C^3) activities, and in the C^3 areas of information sciences and intelligence. The principal technical mission areas are communications, electromagnetic guidance and control, surveillance of ground and aerospace objects, intelligence data collection and handling, information system technology, ionospheric propagation, solid state sciences, microwave physics and electronic reliability, maintainability and compatibility.

AMERICAN REVOLUTION BICENTENNIAL
1776-1976